

Spectroscopy of Eu³⁺-Doped PtS₂ Nanoclusters

F. Parsapour,[†] D. F. Kelley,^{*,†} and R. S. Williams[‡]

Department of Chemistry, Colorado State University, Fort Collins, Colorado 80523-1872, and Hewlett-Packard Laboratories, 3500 Deer Creek Road, MS 26-U, Palo Alto, California 94394-1392

Received: June 15, 1998; In Final Form: August 10, 1998

The synthesis and characterization of PtS₂ nanoclusters synthesized in AOT/hexanol/heptane inverse micelles are reported. Electron diffraction and optical spectroscopy have been used to characterize these nanoclusters. The electron diffraction results show that the nanoclusters have the same crystal structure as bulk PtS₂ and are consistent with the nanoclusters being a single S–Pt–S trilayer. Absorption spectroscopy shows that these nanoclusters have an indirect band gap of 1.58 eV as compared to 0.87 eV for bulk PtS₂. The nanoclusters can be grown such that their mass is doubled, resulting in a band gap of 1.27 eV. PtS₂ nanoclusters doped with 1–5% Eu³⁺ were also synthesized in AOT/hexanol/heptane and tridodecylmethylammonium chloride (TDAC)/hexanol/octane inverse micelles. The m_j structure and relative intensities of Europium emission lines are indicative of the symmetry of the local environment and hence the location of the Eu³⁺ ion. It is concluded that synthesis of doped nanoclusters in TDAC/hexanol/octane results in Eu³⁺ ions that are situated in the near-octahedral holes of the PtS₂ lattice, while an AOT/hexanol/heptane synthesis results in a Eu³⁺ ion on the nanocluster edges. The emission and fluorescence excitation spectra show that 4.0 eV optical excitation of the nanocluster results in energy transfer and subsequent luminescence of the europium dopant. Since the europium excited state is at a higher energy than the band gap, it is concluded that energy transfer to the dopant competes with energy relaxation of the electron/hole pair. Passivation of the nanocluster surface trap states is observed to increase the intensity of europium luminescence, and we conclude that trapping also competes with electron/hole energy relaxation.

Introduction

The optical properties of semiconductor nanoclusters have recently been a subject of great interest. Much of this interest results from their unique size-dependent properties. For example, semiconductor nanoclusters exhibit size dependence of their band gap as a result of quantum confinement of the photogenerated electron/hole pair.¹ This often allows their spectra to be “tuned” over a wide range of wavelengths.

Recently, semiconductor nanoclusters have been explored as potential electroluminescent materials, with applications in optoelectronics.^{2,3} One approach to producing strongly luminescent nanoclusters is to introduce small quantities of an emissive dopant. ZnS nanoclusters have been successfully doped with Mn²⁺, and Mn²⁺ emission has been observed following band gap excitation. This emission has been assigned to the ⁴T₁–⁶A₁ transition of the Mn²⁺ ion,^{4–6} which is excited by energy transfer from the ZnS electron/hole state.

Another interesting class of dopants is the rare earth metal ions. Rare earth ions are excellent fluorophores because of their stability and high emission quantum yields. For example, Eu³⁺ is used to provide red emission in color CRTs. If rare earth ions can be doped into semiconductor nanoclusters, then band gap excitation may result in efficient energy transfer and hence intense luminescence from the rare earth ion. This is particularly true if, through quantum confinement, the band gap state is resonant with an excited state of the rare earth ion. If the band gap state can be produced by electrically injecting electrons and holes, rather than by optical excitation, then rare earth-doped

semiconductor nanoclusters could be made into efficient electroluminescent materials. It is therefore of considerable interest to dope semiconductor nanoclusters with rare earth ions.

In this paper, we report the first synthesis and characterization of PtS₂ nanoclusters and PtS₂ nanoclusters doped with Eu³⁺. PtS₂ crystallizes into the CdI₂ structure (trigonal system, P3 m1). The bulk crystal structural units are composed of platinum atoms in the octahedral holes between close-packed planes of sulfur atoms. The bulk crystal thus consists of covalently bound S–Pt–S trilayers that are held together by van der Waals forces. Previous spectroscopic studies of bulk PtS₂ have elucidated the band gap energies and phonon frequencies.⁷ PtS₂ is an indirect band gap semiconductor with bulk band gaps of 0.95 and 0.87 eV parallel and perpendicular to the trilayers, respectively, at 300 K.⁷ Photoexcitation results in a transition between t_{2g} and e_g type metal orbitals, and because of mostly nonbonding character of these orbitals, PtS₂ is expected to be relatively photostable. Europium spectroscopy is rather complicated but quite well understood.^{8,9} The emission spectrum of Eu³⁺ typically consists of a series of lines in the red (580–700 nm). The most intense emission lines occur at about 592, 612, and 697 nm and are assigned to ⁵D₀ → ⁷F₁, ⁵D₀ → ⁷F₂, and ⁵D₀ → ⁷F₄ transitions, respectively. The m_j structure and relative intensities of these lines are indicative of the Eu³⁺ ion local electric fields. This provides a powerful structural probe of the local environment and thus a diagnostic of the location (interior vs exterior of the nanocluster) of the europium dopant.

Experimental Procedures

PtS₂ nanoclusters are synthesized in inverse micelle solutions, which have been shown to provide a stable environment for semiconductor nanocluster nucleation and growth.¹⁰ The nano-

* To whom correspondence should be addressed.

[†] Colorado State University.

[‡] Hewlett-Packard Laboratories.

clusters are produced by the reaction PtCl_4 and $(\text{NH}_4)_2\text{S}$. Both reagents are dissolved in equal volumes of degassed inverse micelles and rapidly mixed together. Two types of inverse micelles were used in these syntheses and were found to yield indistinguishable nondoped PtS_2 nanoclusters. One type of inverse micelle solution is comprised of a ternary mixture of tridodecylmethylammonium chloride (TDAC)/hexanol/octane with a ratio of 8/8/84 by mass. In a typical preparation of PtS_2 nanoclusters, 6 mL of degassed inverse micelle solution containing 4.5 μL of 22% $(\text{NH}_4)_2\text{S}$ in water is added to 6 mL of a 1.6×10^{-3} M solution of PtCl_4 in inverse micelle (degassed) utilizing the Schlenk technique. The reaction proceeds in a few minutes but is allowed to stir for about 1 h to ensure complete reaction. Alternatively, sodium bis(2-ethylhexyl)sulfosuccinate (AOT) was used as a surfactant, forming either AOT/water/heptane or AOT/hexanol/heptane inverse micelles. The AOT and water concentrations were 1 and 4 M, respectively, while the AOT and hexanol concentrations were 1 and 2 M, respectively. In all cases, the absorption spectrum of the product displayed the loss of the PtCl_4 peak at 272 nm and a broad featureless absorption at wavelengths less than ~ 650 nm. Following synthesis, these nanoclusters may be repeatedly extracted with acetonitrile. Extraction removes the TDAC and hexanol (or AOT and water) while leaving the nanoclusters in the hydrocarbon phase.

Larger nanoclusters are synthesized as follows. First, a solution of small PtS_2 nanoclusters is synthesized in AOT/water/heptane, as described above. To this solution is added a micellar solution of PtCl_4 , having the same number of moles of PtCl_4 as the original micellar solution. An $(\text{NH}_4)_2\text{S}$ micellar solution is then slowly added dropwise. This addition takes about 1 h, and as such, the $(\text{NH}_4)_2\text{S}$ concentration in the $\text{PtS}_2/\text{PtCl}_4$ solution is never high enough to cause nucleation. Similar procedures have previously been used to synthesize other types of composite nanoclusters.¹¹ Following synthesis, these nanoclusters may be repeatedly extracted with acetonitrile.

Synthesis of Eu^{3+} -doped PtS_2 nanoclusters was accomplished in the following ways. First, a solution of 7.7×10^{-4} M EuCl_3 in TDAC/hexanol/octane ternary micelle was prepared under nitrogen atmosphere. A total of 0.2 mL of this solution was added to 6 mL of a 1.6×10^{-3} M PtCl_4 ternary micelle solution, and the same procedure was followed as indicated above. This resulted in the final product containing 1.6% Eu^{3+} ions with respect to the total number of Pt^{4+} ions. Samples have been prepared with Eu^{3+} concentrations between 1 and 5%. Samples were also prepared in an exactly analogous fashion using AOT/hexanol/heptane micelles. The doped nanoclusters showed absorption spectra that are identical to those of the small nondoped nanoclusters plus the Europium ions. In all cases, these nanoclusters were found to be very photostable, showing no detectable degradation after many days of exposure to room lights or several hours of irradiation in the emission spectrometer.

TDAC (Aldrich) was purified using activated charcoal, followed by several recrystallizations from hexane. Octane (Aldrich) and heptane (Aldrich) were purified by distillation off of metallic sodium. Hexanol (Aldrich) was purified by distillation off of iodine-activated magnesium. AOT (Aldrich) was dried by dissolution in diethyl ether with activated molecular sieves. The ether was pumped off following filtration. The resulting dry AOT was found to be free of detectable fluorescent impurities. In all cases, the above materials were monitored for impurities by optical spectroscopy. PtCl_4 (98% Aldrich),

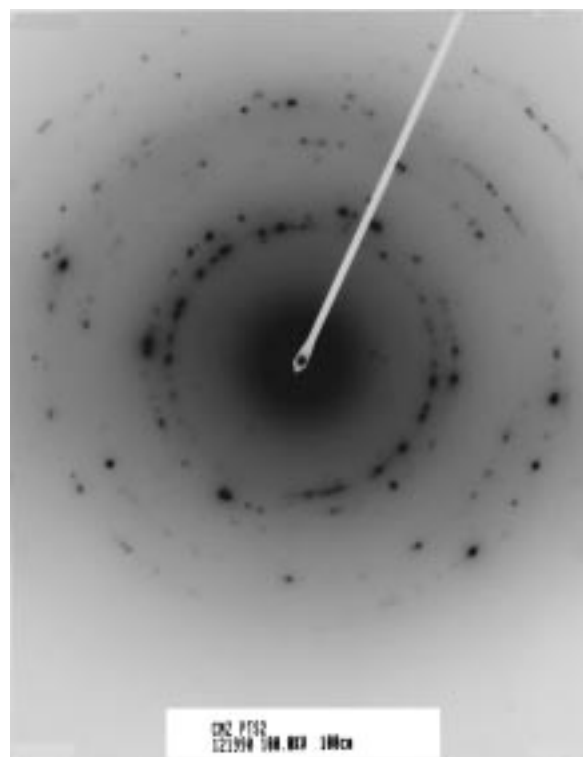


Figure 1. Electron diffraction results from PtS_2 nanoclusters.

$(\text{NH}_4)_2\text{S}$ (22% aqueous solution Aldrich), and EuCl_3 (99.9% Aldrich) were used as received.

Static emission spectroscopy was performed utilizing a home-built fluorometer. The excitation source is the output of a 200-W Hg or a 150-W Hg/Xe lamp through an Oriel 1/8 m double monochromator. Fluorescence from the sample is directed to a 0.65 m ISA monochromator that is coupled to a Hamamatsu R943-02 Ga/As photomultiplier tube with single photon counting electronics. Emission spectra obtained were not corrected for the instrument response; however, the instrument response is fairly flat over the region of interest. Fluorescence excitation spectra were corrected for instrument response. Absorption spectra were obtained using a Hewlett-Packard 5486 diode array spectrophotometer.

Electron diffraction results and TEM images were obtained at the C.S.U. Electron Microscopy Center on a JEOL JEM-2000 electron microscope. Samples used for electron diffraction were prepared by evaporating a 10^{-3} M heptane nanocluster solution on a Formvar/Cu grid. Samples used for TEM imaging were prepared in the same way, except they were a factor of 10 more dilute.

Results and Discussion

PtS_2 Nanoclusters. The electron diffraction powder pattern of PtS_2 nanoclusters is shown in Figure 1. The diffraction pattern shows rings consisting of discrete spots rather than continuous rings. This results from there being a finite number of nanoclusters or nanocluster aggregates on the irradiated surface. The center-to-ring diffraction angles, relative to the (1,0,0) reflection, are collected in Table 1. Literature values¹² and their assignments are also collected in Table 1. There is a one-to-one correspondence between the observed diffraction rings and those reported in the literature, with the exception of the (0,0,1), (0,0,2), and (0,0,4) reflections (discussed below). There is also excellent agreement between the observed diffraction angles and the literature data, establishing that the nanoclusters have the same crystal structure as bulk PtS_2 .

TABLE 1: Electron Diffraction Results

crystallographic assignment	relative displacement ¹² (sin θ)	observed relative displacement ^a (sin θ)
(0,0,1)	0.608	not observed
(1,0,0)	1.00	1.00 (s)
(1,0,1)	1.17	1.14 (s)
(0,0,2)	1.21	not observed
(1,0,2)	1.57	1.63 (s)
(1,1,0)	1.73	1.70 (vw)
(1,1,1)	1.83	1.90 (s)
(2,0,0)	2.00	2.00 (w)
(1,0,3)	2.08	2.06 (w)
(1,1,2)	2.11	2.10 (w)
(2,0,2)	2.34	2.35 (w)
(0,0,4)	2.43	not observed
(1,1,3)	2.51	2.51 (w)

^a Intensities are given by the following abbreviations: strong (s), weak (w), very weak (vw).

The electron diffraction results also bear on the nanocluster morphology. We note that the reflections associated with only the *c*-axis, specifically the (0,0,1), (0,0,2), and (0,0,4), are absent in the observed electron diffraction pattern. This indicates that there is no long-range periodicity along the *c*-axis. The crystallographic *c*-axis is perpendicular to the planes associated with the S–Pt–S trilayers in bulk PtS₂. The electron diffraction pattern is therefore consistent with the nanoclusters being two-dimensional, specifically consisting of a single or a few trilayers. The single trilayer morphology is expected for the following reason. Following nucleation, the nanoclusters are expected to grow by the addition of Pt and S at the reactive trilayer edges. Growth along the *c*-axis corresponds to further nucleation and should therefore be relatively slow. This single trilayer, disk morphology has been observed in preliminary STM images of MoS₂ nanoclusters, which also has a layered crystal structure. STM studies of PtS₂ nanoclusters will definitively establish the morphology of these nanoclusters. These studies are in progress and will be reported in a later paper.

The absorption spectrum for PtS₂ nanoclusters is shown in Figure 2. A broad absorption with an onset near 500 nm is observed for the PtS₂ nanoclusters, which is absent in the absorption spectrum of the PtCl₄ and (NH₄)₂S reactants. In addition, an intense peak at 272 nm, which is assigned to PtCl₄, is absent from the nanocluster spectrum. Bulk PtS₂ also shows a diffuse, unresolved spectrum, the onset of which is assigned to the indirect transition. An estimate of the indirect band gap may be obtained from these featureless absorption spectra. Band gap estimates for indirect semiconductors are obtained from a plot of $\epsilon_2^{1/2}$ versus energy, where ϵ_2 is the imaginary part of the dielectric constant.^{7,13} ϵ_2 is often approximated as being proportional to the absorption coefficient, and extrapolation to zero absorbance gives the energy of the band gap plus the phonon involved in the indirect transition. This analysis for bulk PtS₂ gives a band gap energy of about 0.87 eV for absorption perpendicular to the *c*-axis and 0.95 eV for the absorption to parallel to the *c*-axis. A corresponding plot of $A^{1/2}$ versus energy is also shown in Figure 2. (In both the bulk and nanocluster cases, a very weak, wavelength-independent absorption due to trap states is subtracted off.) We deduce a band gap of about 1.58 eV for the smaller (initial) nanoclusters and a band gap of about 1.27 eV following the cluster growth procedure explained in the Experimental Section. The band gap energies of the smaller and larger nanoclusters are about 0.71 and 0.40 eV, respectively, larger than the perpendicular absorption bulk band gap. The growth procedure should double the mass of the nanoclusters while lowering their number density

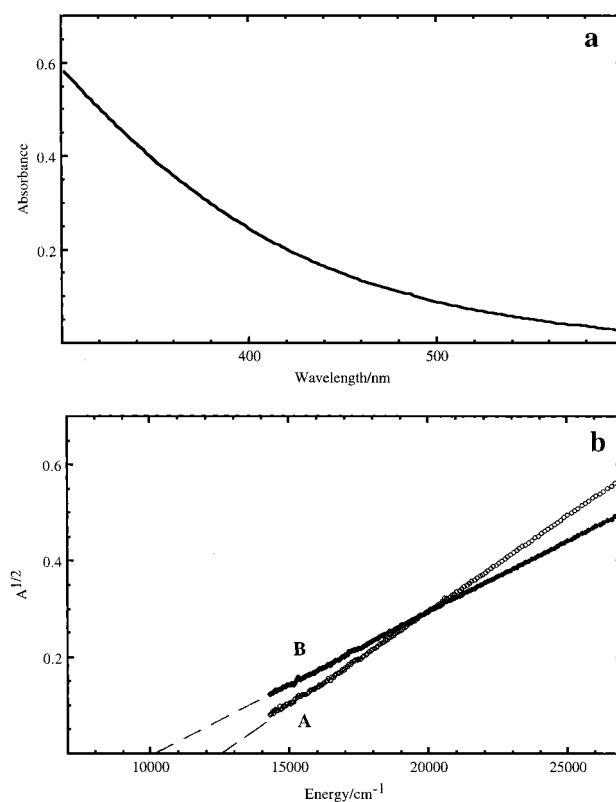


Figure 2. (a) Absorption spectrum of PtS₂ nanoclusters. (b) Plot of square root of absorbance vs energy for PtS₂ nanoclusters. The extrapolations of $A^{1/2}$ to zero give values of 12 850 and 10 300 cm^{-1} for the initially formed (A) and subsequently grown nanoclusters (B), respectively.

by a factor of 2. Assuming that the nanoclusters form single-trilayer disklike structures, the diameter of the larger ones should therefore be a factor of $\sqrt{2}$ larger than that of the smaller ones. This result is in approximate agreement with the predictions of “effective mass” theories of quantum confinement. Simple quantum confinement theory¹ predicts that the shift of the band gap from the bulk value should be approximately proportional to (diameter)⁻². Thus, it is predicted that quantum confinement band gap shift should be about twice as large in the small nanocluster case. As indicated above, values of 0.40 and 0.71 eV are obtained, in approximate agreement with this prediction. The production of larger nanoclusters from the smaller ones is important because it unambiguously shows that PtS₂ nanoclusters have indeed been synthesized.

Ideally, these nanoclusters would be characterized by TEM, revealing the size distribution of each sample. However, obtaining TEM images of PtS₂ nanoclusters is somewhat problematic. This is because PtS₂ decomposes at about 225 °C. Current densities must therefore be kept very low to prevent local heating beyond this limit. As a result, only low contrast TEM images could be obtained. Despite this difficulty, a few TEM images of the smaller (indirect band gap of 1.58 eV) particles have been obtained. While these images show particle diameters of about 60 Å, it is impossible to know if these images are characteristic of the sample as a whole. Thus, we do not know if this reflects the average particle size and can make no estimate of the distribution of cluster sizes. We emphasize, however, that the focus of this paper is the doping of the nanoclusters with europium ions and that the size distribution is not important in the present study.

Eu³⁺ Spectroscopy. The emission spectrum of EuCl₃ at a concentration of 4×10^{-7} M in an AOT/hexanol/heptane

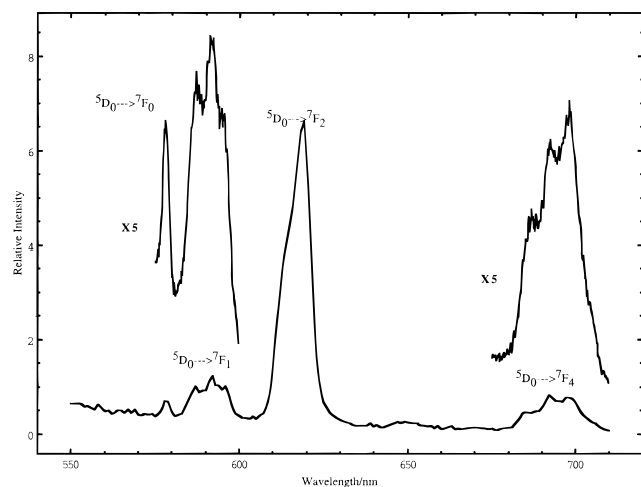


Figure 3. Dispersed emission spectrum of 4×10^{-7} M EuCl_3 in AOT/hexanol/heptane inverse micelles.

micelle is shown in Figure 3. The spectrum consists of a series of well-resolved features at 578, 592, 618, and 698 nm, which are assigned to $^5\text{D}_0 \rightarrow ^7\text{F}_J$, $J = 0, 1, 2, 4$, transitions, respectively. Each of these peaks is partially resolved into the various m_J transitions. This emission spectrum can reveal much about the local environment of the Eu^{3+} ion. The selection rules make the $^5\text{D}_0 \rightarrow ^7\text{F}_1$ and $^5\text{D}_0 \rightarrow ^7\text{F}_2$ transitions of particular interest. We will focus on the m_J structure in the $^5\text{D}_0 \rightarrow ^7\text{F}_1$ peak and the $(^5\text{D}_0 \rightarrow ^7\text{F}_2)/(^5\text{D}_0 \rightarrow ^7\text{F}_1)$ intensity ratio.

The extent to which the $^7\text{F}_1$ m_J levels are split depends on magnitude and symmetry of the local electric field. The $J = 1$ m_J functions transform as T_1 in cubic symmetry¹⁴ (i.e., they are triply degenerate) and are split in lower symmetry point groups.¹⁵ Since all three m_J peaks are clearly observed, we conclude that in the AOT inverse micelle the Eu^{3+} local symmetry must be D_2 or lower. The splittings observed in the $J = 1$ peak of Figure 3 are fairly large, on the order of 150 cm^{-1} . This indicates the presence of rather large local electric fields. The fact that the m_J peaks are partially resolved indicates only moderate inhomogeneous broadening, roughly comparable to the splittings. The above considerations suggest that in these micelles most of the Eu^{3+} ions are in similar environments, probably bound to the anionic AOT surfactant. Consistent with this conclusion, a relatively strong $^5\text{D}_0 \rightarrow ^7\text{F}_0$ transition is observed at 578 nm. This transition becomes allowed only through “J-mixing”. The exact mechanisms of J-mixing are not completely understood,⁸ but group theory requires that this transition can have finite oscillator strength in point groups in which the dipole moment operator transforms as the totally symmetric representation. This occurs only in the low symmetry groups, specifically C_1 , C_s , and C_n .

The relative intensities of the $^5\text{D}_0 \rightarrow ^7\text{F}_1$ and $^5\text{D}_0 \rightarrow ^7\text{F}_2$ emission lines also provide a probe to the local environment of the Eu^{3+} ion, because the intensities of these transitions depend on the local environment in different ways. To understand the variation of these intensities, we must briefly digress into relevant theory of the selection rules. All of these emission lines correspond to $f-f$ transitions and are nominally electric dipole forbidden. However, in some cases, the nonspherical local environment can mix in other transitions, resulting in finite oscillator strength. The $^5\text{D}_0 \rightarrow ^7\text{F}_1$ transition at $\sim 592 \text{ nm}$ is electric dipole forbidden in all cases and gets intensity from the magnetic dipole operator.⁸ The intensity of this transition is almost completely unaffected by the local environment. By mixing with higher lying allowed transitions, the $^5\text{D}_0 \rightarrow ^7\text{F}_2$

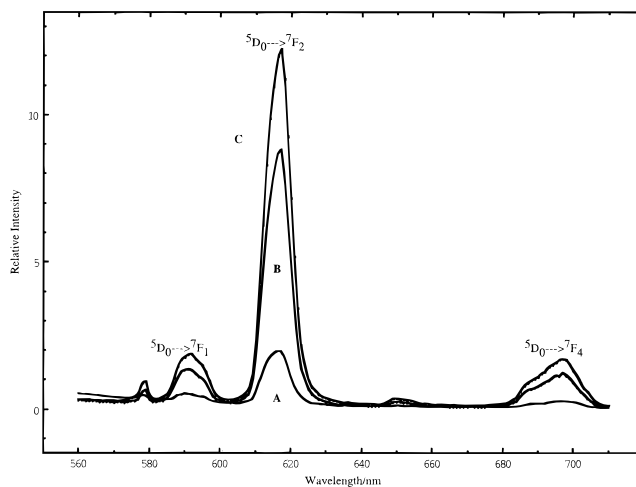


Figure 4. Dispersed emission spectra of (A) EuCl_3 (2×10^{-5} M)/ PtCl_4 (1×10^{-3} M) reactants in AOT/hexanol/heptane, (B) same as A but following the addition of $(\text{NH}_4)_2\text{S}$ in micelle solution, and (C) same as B but following the addition and phase separation of a small amount of acetonitrile. In all cases, excitation is at 312 nm.

transition is electric dipole allowed, and its intensity may be understood in terms of Judd–Ofelt theory.^{8,9} The $^5\text{D}_0 \rightarrow ^7\text{F}_2$ transition is “hypersensitive”, i.e., the extent to which it is electric dipole allowed depends on the local electric field and, hence, the local symmetry. The hypersensitive transition becomes first-order allowed in Judd–Ofelt theory if the local symmetry conforms to any of the following point groups: C_s , C_1 , C_2 , C_3 , C_4 , C_6 , C_{2v} , C_{3v} , C_{4v} , and C_{6v} . This selection rule corresponds to the local electric field having a Y_{1m} spherical harmonic component. The hypersensitive transition may also become allowed through a “dynamic coupling” mechanism.⁸ In the context of Judd–Ofelt theory, this mechanism corresponds to a perturbation treatment in which the polarizability of the surrounding media is considered. If the local electric field has a Y_{3m} component, then finite oscillator strength will result from this mechanism. The transition becomes allowed in the following point groups: C_5 , C_7 , C_8 , C_{5v} , $C_{\infty v}$, C_{3h} , D_2 , D_3 , D_4 , D_5 , D_6 , D_{2d} , D_{3h} , S_4 , T , and T_d . It is important to note that the $^5\text{D}_0 \rightarrow ^7\text{F}_2$ transition remains electric dipole forbidden in octahedral, O_h symmetry. From these considerations it is clear that the $(^5\text{D}_0 \rightarrow ^7\text{F}_2)/(^5\text{D}_0 \rightarrow ^7\text{F}_1)$ intensity ratio can yield information about the local Eu^{3+} environment and will allow us to comment on the location of the Eu^{3+} ions in the doped nanoclusters, below.

Eu^{3+} -Doped PtS_2 Nanoclusters. Micellar solutions of the PtCl_4 and $(\text{NH}_4)_2\text{S}$ reactants as well as the PtS_2 nanoclusters show little or no visible emission, independent of excitation wavelength. However, the addition of EuCl_3 to the PtCl_4 reactant results in an emission spectrum similar to that shown in Figure 3. The emission spectra of the $\text{PtCl}_4/\text{EuCl}_3$ reactants and the nanocluster products are shown in Figure 4. Comparison of the EuCl_3 spectrum in the presence (Figure 4A) and absence (Figure 3) of PtCl_4 shows that the PtCl_4 results in some broadening and loss of the m_J structure in the $^5\text{D}_0 \rightarrow ^7\text{F}_1$ transition. The broadening is due to the presence of large electric fields associated with the Pt^{4+} in the immediate vicinity of the Eu^{3+} ion. The same effect is observed with the addition of any multiply charged metal ion or by simply raising the Eu^{3+} concentration. Addition of a micellar solution of $(\text{NH}_4)_2\text{S}$ results in the product spectrum, shown in Figure 4B. There are several aspects of these spectra along with other observations that indicate that Eu^{3+} -doped PtS_2 nanoclusters have been formed. Specifically, it is of interest to note the intensities of the Eu^{3+}

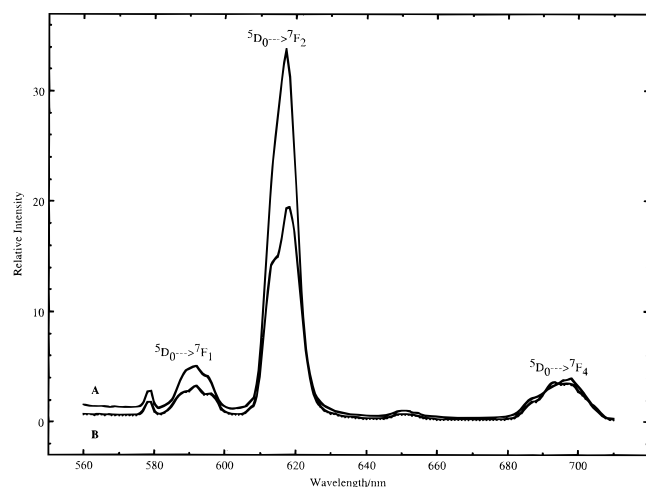


Figure 5. Dispersed emission spectra of (A) EuCl₃ (2×10^{-5} M) in AOT/hexanol/heptane and (B) same as A but following the addition of (NH₄)₂S in micelle solution. In both cases, excitation is at 312 nm.

peaks in the reactant versus product spectra, Figure 4, panels A and B, respectively. The intensities are a factor of approximately 5 greater in the product spectrum, despite the fact that total europium concentration is lower by a factor of 2. (Recall that this factor of 2 dilution occurs because reaction occurs when equal volumes of PtCl₄/EuCl₃ and (NH₄)₂S micellar solutions are mixed.) This observation indicates that the Eu³⁺ ions are more efficiently excited and/or luminesce with a higher quantum yield in the product case. This result may be compared to that obtained in the control experiment, in which no PtCl₄ is present in the reactant mixture, as shown in Figure 5. In this case there is also a factor of 2 dilution and a corresponding factor of 2 drop in the emission intensities. In all cases, the excitation is at 312 nm. The factor of 10 difference between these two cases may be understood in terms of the 312-nm absorption intensities. The absorption spectrum produced by the reaction of PtCl₄/EuCl₃ with (NH₄)₂S is a superposition of the weak Eu³⁺ absorptions and the PtS₂ nanocluster spectrum (Figure 2), which exhibits a strong absorption at 312 nm. In contrast, the sample produced without PtCl₄ has very little absorbance at 312 nm. This difference may also be seen in the europium excitation spectra. The fluorescence excitation (FE) spectra obtained when observing the Eu³⁺ ⁵D₀ → ⁷F₂ (618 nm) transition are shown in Figure 6. The 300–420-nm FE spectrum of the PtCl₄/EuCl₃ reactants shows a weak Eu³⁺ absorption line at 394 nm that is assigned to the ⁷F₀ → ⁵L₆ transition and an unresolved absorption having somewhat greater intensity at wavelengths below 330 nm. The latter absorption may be assigned to transitions to several ⁵H and ⁵F states in that energy range. A very similar result is obtained in the EuCl₃/(NH₄)₂S product spectrum. The product PtCl₄/EuCl₃/(NH₄)₂S (doped nanocluster) FE spectrum consists of this same 394-nm line and a much more intense featureless absorption that starts at about 330 nm and increases at shorter wavelengths. This broad absorption is partially due to direct absorption of the Eu³⁺ ion but is primarily assigned to the PtS₂ nanoclusters.¹⁷ The FE spectrum in Figure 6B is not expected to match the PtS₂ nanocluster absorption spectrum for the following reason. The Eu³⁺ ⁵D₀ state may excited directly by energy transfer from the nanocluster or energy transfer to higher lying states followed by relaxation to the ⁵D₀ state. All of these states are above the PtS₂ nanocluster band gap and therefore may be excited only by unrelaxed electron/hole pairs. Thus, efficient excitation of the Eu³⁺ ion occurs only when the photon energy is greater

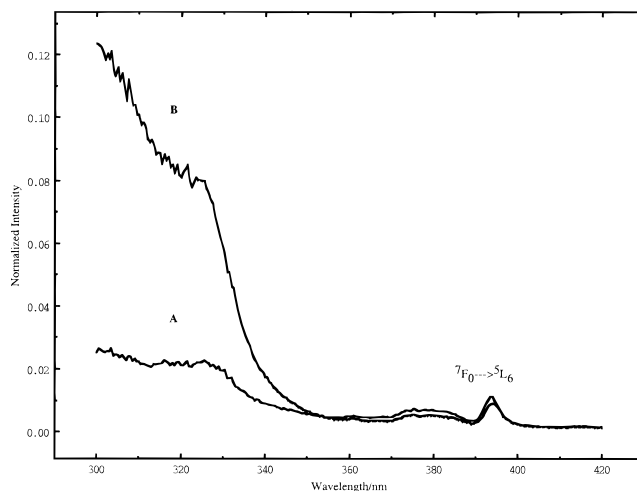


Figure 6. Fluorescence excitation spectra of (A) EuCl₃ (2×10^{-5} M)/PtCl₄ (1×10^{-3} M) reactants in AOT/hexanol/heptane and (B) same as A but following the addition of (NH₃)₂S micelle solution. The observation wavelength was 618 nm.

than the excitation energy of the states that most strongly couple to the nanocluster electron/hole pair. In this case, energy transfer to the Eu³⁺ ion competes with electron and hole relaxation. (The dynamics of this competition are discussed in the next section.) These considerations suggest that the ⁵H and ⁵F states strongly couple to the electron/hole pair and that energy transfer to yield these states (and finally the emissive ⁵D₀ state) is efficient only when the photon energy is at or above their excitation energies, specifically at wavelengths below 330 nm. Figure 6B shows significant intensity only below about 340 nm, in accord with this assignment. In addition to nanocluster to rare earth energy transfer, the small band gap of these nanoclusters makes the reverse process possible. Thus, the observed factor of 10 increase in emission intensity reflects a lower limit in the increase in excitation efficiency.

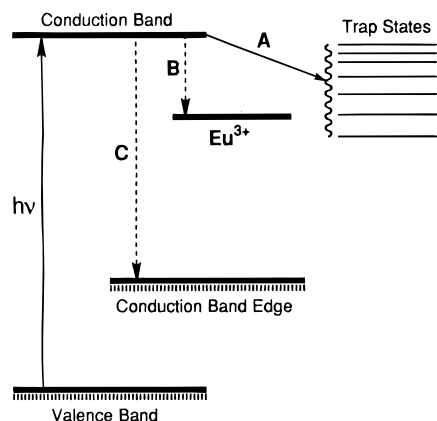
The above spectra yield an important conclusion: excitation of the PtS₂ nanoclusters with 300–420-nm light results in excitation of the europium ions. This implies nanocluster to rare earth energy transfer, which is expected to be efficient only if the Eu³⁺ is in contact with the nanocluster. Thus, these spectra indicate the Eu³⁺ ions are intimately associated with the PtS₂ nanoclusters, either in the interior or on the nanocluster surface.

The above conclusion is consistent with the results of O₂ and H₂O quenching studies. The presence of small amounts of O₂ significantly quenches the emission of Eu³⁺ in solution. Specifically, the emission intensity of Eu³⁺ in ternary AOT micelle is diminished by a factor of ~4 upon exposure to atmospheric oxygen. Subsequent degassing of the solution returns the emission to its original intensity. The quenching probably occurs by energy transfer from the Eu³⁺ ⁵D₀ state to form singlet oxygen. No oxygen quenching is observed following reaction with (NH₄)₂S in either the PtCl₄/EuCl₃/(NH₄)₂S or EuCl₃/(NH₄)₂S cases. In the former case, Eu³⁺-doped PtS₂ nanoclusters are formed, while in the latter case small particles of europium sulfide are formed. These particles probably consist of the sesquisulfide, Eu₂S₃, in analogy with other rare earths.¹⁶ In both cases, the presence of the surrounding sulfide ions prevents O₂ quenching.

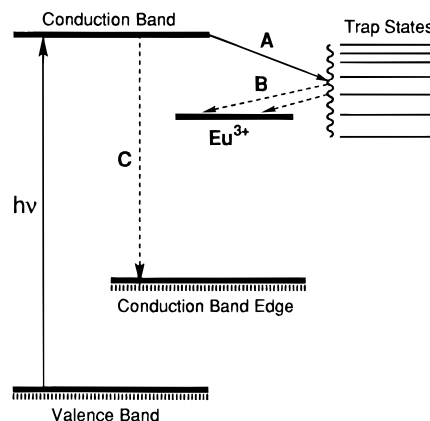
H₂O also quenches the ⁵D₀ state by energy transfer to the O–H stretch modes. Addition of 0.2 M H₂O to a solution of EuCl₃ in ternary AOT micelle quenches the Eu³⁺ emission by a factor of ~6.2. Much less quenching is observed in the EuCl₃/

SCHEME 1

Mechanism I



Mechanism II



(NH₄)₂S (probably Eu₂S₃ particles) case; about a factor of 2.0. This is because most of the Eu³⁺ ions are in the particle interior and inaccessible to the H₂O. The Eu³⁺-doped PtS₂ nanocluster consists of a single S–Pt–S trilayer as discussed above. Thus, a dopant on the interior or edge is only a single sulfide away from the H₂O molecules and may be effectively quenched. Consistent with this expectation, quenching of about a factor of 4.7 is observed in this case.

The doped nanocluster europium emission spectra presented in Figure 4 allowed us to comment on the location of the Eu³⁺ ions in the PtS₂ nanocluster. The PtCl₄/EuCl₃ reactant spectrum shows considerable m_j splitting in the ⁵D₀ → ⁷F₁ peak, as discussed above. This is indicative of strong local electric fields of low symmetry at the Eu³⁺ ions. Consistent with this observation, a large (⁵D₀ → ⁷F₂)/(⁵D₀ → ⁷F₁) intensity ratio of about 8.3 is observed. The Eu³⁺-doped PtS₂ nanocluster spectrum is more intense but shows a *J* = 1 peak of comparable width and a similar (⁵D₀ → ⁷F₂)/(⁵D₀ → ⁷F₁) intensity ratio. This suggests that the Eu³⁺ ions are in low symmetry sites. The two most obvious possible Eu³⁺ locations are at the nanocluster edge or substituted for Pt⁴⁺ ions in the nanocluster interior. In the latter case, the Eu³⁺ ions would be situated in the octahedral holes between the planes of close-packed sulfur ions. However, in octahedral symmetry, the ⁵D₀ → ⁷F₂ transition is completely forbidden and the (⁵D₀ → ⁷F₂)/(⁵D₀ → ⁷F₁) ratio is expected to diminish. The large ratio observed in these spectra therefore suggests that the Eu³⁺ ions are at the nanocluster edges.

The above results may be compared with those obtained from doped nanoclusters synthesized in TDAC/hexanol/octane inverse micelles. The emission spectrum of the PtCl₄/EuCl₃ reactant mixtures is shown in Figure 7. This spectrum has two significant differences as compared to the analogous spectrum in AOT/hexanol/heptane (see Figure 4). First, the ⁵D₀ → ⁷F₁ peak is considerably narrower with no resolved m_j structure. Second the (⁵D₀ → ⁷F₂)/(⁵D₀ → ⁷F₁) intensity ratio is not as large, about 6.1. Both of these observations indicate the absence of strong local electric fields in the TDAC/hexanol/octane micelles. Reaction with (NH₄)₂S, followed by extraction with acetonitrile, results in a considerably different spectrum, also shown in Figure 7. In this case, the ⁵D₀ → ⁷F₁ peak is slightly narrower, with no indication of resolved m_j structure. Also, the (⁵D₀ → ⁷F₂)/(⁵D₀ → ⁷F₁) intensity ratio is dramatically reduced, to about 2.0, suggesting that the ⁵D₀ → ⁷F₂ transition is now strongly forbidden. We also note that the ⁵D₀ → ⁷F₀ transition is completely absent in these spectra. From these observations, we conclude that following reaction the Eu³⁺ ions are in the

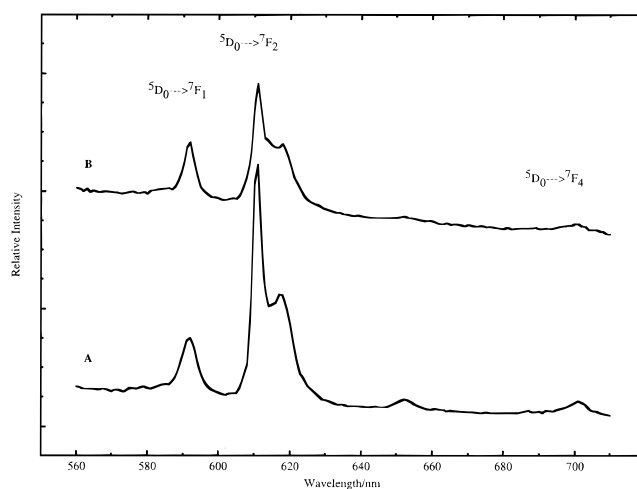


Figure 7. Dispersed emission spectra of (A) EuCl₃ (2×10^{-5} M)/PtCl₄ (1×10^{-3} M) in TDAC/hexanol/octane inverse micelles and (B) same as A but following the addition of (NH₄)₂S in TDAC/hexanol/octane micelle. In both cases, excitation is at 312 nm.

interior octahedral holes of the PtS₂ lattice. Based on the bulk crystal structures, these holes have radii of about 0.75 Å, which is somewhat less than the 0.95 Å ionic radius of a Eu³⁺ ion, and the environment is not expected to remain strictly octahedral. This may explain why some intensity is retained in the ⁵D₀ → ⁷F₂ transition.

We suggest that the difference in Eu³⁺ location resulting from these two different synthetic environments may be due to different Eu³⁺ reactivities. In the AOT micelles, the Eu³⁺ is fairly strongly associated with the anionic AOT surfactant, as indicated by emission spectrum shown in Figure 3. This may reduce the reactivity of the Eu³⁺ ions, with the result being that they react with the sulfide much more slowly than nanocluster formation. The result is comparatively rapid nanocluster formation, followed by europium reaction onto the nanocluster edges. No strong association occurs on the cationic TDAC micelles, and in this case the europium reactivity is much greater. We suggest that, in this case, europium reaction with the sulfide occurs along with nanocluster formation and that europium is incorporated into the nanocluster.

Energy Transfer Dynamics. The overall quantum yield for europium emission in these nanoclusters is quite low, 10^{-4} – 10^{-5} , suggesting that energy transfer from the PtS₂ e⁻/h⁺ state to the Eu³⁺ dopant atoms is inefficient. This is not too surprising, considering that the upper level for emission (⁵D₀)

is at an energy of 2.14 eV, while the nanocluster band gap is 1.58 eV. The excitation energy of the spectra presented in Figure 4 is 3.97 eV, and as mentioned above, energy transfer to the europium must compete with electron relaxation to the bottom of the conduction band and/or hole relaxation to the top of the valence band. Two energy relaxation pathways can be suggested and are depicted in Scheme 1. In mechanism I, energy relaxation (C) competes with both electron and/or hole trapping (A) as well as energy transfer to the Eu³⁺ dopant (B). Subsequent energy transfer from the trap states is considered to be unimportant. The opposite situation is considered in mechanism II. In this case, it is assumed that energy transfer occurs primarily from the trap states (B) and that energy transfer from the unrelaxed electron/hole pairs in the conduction/valence bands is unimportant. These two limiting-case mechanisms may be distinguished by removing some fraction of the trap states and observing the change in europium emission intensity. Removing some of the trap states will have the effect of slowing the rate of trapping. In the case of mechanism I, this will result in an increase of the europium emission, while the opposite is true for mechanism II.

In these small nanoclusters, most trap states are probably associated with surface or edge dangling bonds, as has been shown to be the case in other types of semiconductor nanoclusters.^{18,19} These dangling bonds may be partially eliminated and the traps passivated by reaction with an electron-donating species, such as a nitrile. In the present case, this is accomplished by extracting the nanocluster/inverse micelle solution with acetonitrile. Addition of acetonitrile to nanocluster/inverse micelle solution results in phase separation with disruption of the inverse micelles. The TDAC or AOT surfactant and hexanol go into the acetonitrile phase, while the doped PtS₂ nanoclusters are observed to stay in the octane phase. This does not result in any change in the nanocluster absorption spectrum, indicating that no precipitation or aggregation has occurred. The absence of aggregation indicates that some acetonitrile has indeed been adsorbed onto the reactive edges. The result of acetonitrile extraction on the emission spectrum is shown in Figure 4. A significant increase in the europium emission intensity is observed. It could be argued that the high frequency hexanol OH stretch mode partially quenches the europium emission and that the observed increase in intensity is due to removal of hexanol. However, subsequent addition of more hexanol following acetonitrile extraction has no effect on the emission intensity, indicating that the increase is due to trap passivation caused by the acetonitrile. We conclude that the dominant pathway leading to excited state europium is depicted in mechanism I. These studies suggest that if the band gap energy were equal to or greater than the rare earth excitation energy, much more efficient energy transfer might occur. Studies aimed at examining this situation are currently in progress.

Conclusions

The central conclusions of this work are summarized below.

(1) PtS₂ nanoclusters may be nucleated and subsequently grown in size, using inverse micelle techniques. The dependence of the absorption spectrum on nanocluster size may be semiquantitatively understood in terms of simple quantum confinement theory.

(2) Electron diffraction results indicate that the nanoclusters are single or possibly a few S–Pt–S trilayer disks, which are essentially fragments of the planar trilayers that comprise the bulk semiconductor material.

(3) Eu³⁺ ions may be doped into PtS₂ nanoclusters by including a few percent of EuCl₃ into the nanocluster synthesis. The Eu³⁺ ions may reside either on the nanocluster edges or in the octahedral holes of the PtS₂ lattice depending upon the synthetic conditions. This structural conclusion is established by analysis of the m_j structure in the ⁵D₀ → ⁷F₁ transition and the relative intensities of Eu³⁺ emission lines using the Judd–Ofelt theory.

(4) Dopant Eu³⁺ ions may be excited by an energy transfer mechanism, following excitation above the nanocluster band gap. Energy transfer to surface trap states competes with energy transfer to dopant ions.

Acknowledgment. This work was supported by a grant from the Department of Energy, Contract DE-FG03-96ER14717. The authors would also like to thank Ms. C. Zelenski and Prof. P. K. Dorhout for their help with the electron diffraction results.

References and Notes

- (1) For reviews, see (a) *Semiconductor Nanoclusters—Physical, Chemical and Catalytic Aspects*; Kamat, P. V., Meisel, D., Eds.; Elsevier: Amsterdam, 1997. (b) Alivasatos, A. P. *J. Phys. Chem.* **1996**, *100*, 13226. (c) Steigerwald, M. L.; Brus, L. E. *Annu. Rev. Mater. Sci.* **1989**, *19*, 147. (d) Yoffe, A. D. *Adv. Phys.* **1993**, *42*, 173. (e) Brus, L. E. *J. Chem. Phys.* **1983**, *79*, 5566; **1984**, *80*, 4403. (f) Brus, L. E. *J. Phys. Chem.* **1986**, *90*, 2555.
- (2) (a) Colvin, V. L.; Schlamp, M. C.; Alivisatos, A. P. *Nature* **1994**, *370*, 354. (b) Greenham, N. C.; Peng, X.; Alivisatos, A. P. *Phys. Rev. B* **1996**, *54*, 17628.
- (3) Dabbousi, B. O.; Bawendi, M. G.; Onitsuka, O.; Rubner, M. F. *Appl. Phys. Lett.* **1995**, *66*, 1316. (b) Danek, M.; Jensen, K. F.; Murray, C. B.; Bawendi, M. G. *Chem. Mater.* **1996**, *8*, 173.
- (4) Bhargava, R. N.; Gallagher, D.; Welker, T. *J. Lumin.* **1994**, *60*, 275.
- (5) (a) Gallagher, D.; Heady, W. E.; Racz, J. M.; Bhargava, R. N. *J. Mater. Res.* **1995**, *10*, 870. (b) *J. Cryst. Growth* **1994**, *138*, 970. (c) Bhargava, R. N.; Gallagher, D.; Ilong, X.; Nurmikko, A. *Phys. Rev. Lett.* **1994**, *72*, 416.
- (6) Sooklal, K.; Michael, B. S.; Angel, S. M.; Murphy, C. J. *J. Phys. Chem.* **1996**, *100*, 4551.
- (7) Mankai, C.; Martinez, G.; Gorochov, O. *Phys. Rev. B* **1977**, *16*, 4666.
- (8) Peacock, R. D. In *Structure and Bonding*; Springer-Verlag: New York, 1975; Vol. 22, pp 83–122.
- (9) (a) Judd, B. R. *Phys. Rev.* **1962**, *127*, 750. (b) Ofelt, G. S. *J. Chem. Phys.* **1962**, *37*, 511.
- (10) (a) Petit, C.; Lixon, P.; Pileni, M. P. *J. Phys. Chem.* **1990**, *94*, 1598. (b) Petit, C.; Pileni, M. P. *J. Phys. Chem.* **1988**, *92*, 2282. (c) Modes, S.; Lianos, P. *J. Phys. Chem.* **1989**, *93*, 5854. (d) Lianos, P.; Thomas, J. K. *J. Colloid Interface Sci.* **1987**, *117*, 505. (e) Lianos, P.; Thomas, J. K. *Chem. Phys. Lett.* **1986**, *125*, 299. (f) Kuczynski, J.; Thomas, J. K. *Langmuir* **1985**, *1*, 158.
- (11) (a) Kortan, A. R.; Hull, R.; Opila, R. L.; Bawendi, M. G.; Steigerwald, M. L.; Carrol, P. J.; Brus, L. E. *J. Am. Chem. Soc.* **1990**, *112*, 1327. (b) Eychmuller, A.; Mews, A.; Weller, H. *Chem. Phys. Lett.* **1993**, *208*, 59. (c) *Phys. Rev. B* **1996**, *53*, 13242.
- (12) (a) Finley, A.; Schliech, D.; Ackermann, J.; Soled, S.; Wold, A. *Mater. Res. Bull.* **1974**, *9*, 1655. (b) Gronvold; Haraldson; Kjekshas *Acta Chem. Scand.* **1960**, *14*, 1879.
- (13) Boer, K. W. *Survey of Semiconductor Physics*; Van Nostrand Reinhold: New York, 1990; Chapter 13.
- (14) Abragam, A.; Bleaney, B. In *Electron Paramagnetic Resonance of Transition Metal Ions*; Oxford Press: Oxford, 1970; Appendix B.
- (15) Wilson, E. B.; Decius, J. C.; Cross, P. C. In *Molecular Vibrations*; Dover: New York, 1955; Appendix X-8.
- (16) Chen, J. H.; Dorhout, P. K. *J. Solid State Chem.* **1995**, *117*, 318.
- (17) The possibility that the increased absorption is due to electrodynamic effects of the nanocluster increasing the rare earth absorption may also be considered. See Wang, Y.; Herron, N. *J. Phys. Chem.* **1991**, *95*, 525. However this explanation would not account for the observed rapidly increasing intensity in the 320–300-nm region, making this assignment unlikely.
- (18) (a) Dannhauser, T.; O'Neil, M.; Johansson, K.; Whitten, D.; McLendon, G. *J. Phys. Chem.* **1986**, *90*, 6074; (b) Spanhel, L.; Haase, M.; Weller, H.; Henglein, A. *J. Am. Chem. Soc.* **1987**, *109*, 5649.
- (19) Doolen, R.; Laitinen, R.; Parsapour, F.; Kelley, D. F. *J. Phys. Chem. B* **1998**, *102*, 3906.